ELECTRON TRANSPORT MODEL OF DIELECTRIC CHARGING*

Brian L. Beers, Hsing-chow Hwang,
Dong L. Lin, and Vernon W. Pine
SCIENCE APPLICATIONS, INC.

SUMMARY

A computer code (SCCPOEM) has been assembled to describe the charging of dielectrics due to irradiation by electrons. The primary purpose for developing the code was to make available a convenient tool for studying the internal fields and charge densities in electron-irradiated dielectrics. The code, which is based on the primary electron transport code POEM (ref. 1), is applicable to arbitrary dielectrics, source spectra, and current time histories. The code calculations are illustrated by a series of semi-analytical solutions. Calculations to date suggest that the front face electric field is insufficient to cause breakdown, but that bulk breakdown fields can easily be exceeded.

INTRODUCTION

One of the major concerns generated by the spacecraft charging problem is the possibility of catastrophic breakdown and discharge of dielectrically stored charge. By this time, ample experimental evidence is available to indicate that such discharges do occur both in space (see, e.g., refs. 2-3) and in laboratory simulations (see, e.g., refs. 4-12) of the electron charging environment. While it is generally acknowledged that an understanding of these events requires a knowledge of the internal fields and charge densities in the dielectric, very little work on this problem has been reported in the spacecraft charging literature, the notable exceptions being the paper of Meulenberg (ref. 12) and certain estimates reported in the NASCAP code documentation (ref. 13). It is the purpose of this paper to describe our initial research in developing tools for quantitatively understanding these important internal quantities.

*This work was sponsored, in part, by the COMMUNICATIONS RESEARCH CENTRE of Canada.

The general subject of charge trapping, charge storage, and current flow in dielectrics is an exceedingly complex area of research (see, e.g., refs. 14-16). Our approach to this problem for the situations of interest to satellite charging has been to develop a computer model (SCCPOEM) (ref. 17) of the dielectric charging process which

- isolates the essential features of the charging process which depend on the dielectric
- is sufficiently general to permit comparison to laboratory simulation data
- is sufficiently general to permit easy application to arbitrary dielectrics, electron source spectra, and current time histories
- incorporates in a detailed quantitative fashion all those features of the charging process which are believed to be well-known
- has the flexibility to add modular units which may be necessary to describe additional physics
- is inexpensive enough to run to permit parametric studies

To achieve these goals, we have restricted the model to one-dimensional geometry and have coupled the existing SAI Monte Carlo electron transport code POEM (ref. 1) with various standard algorithms for computing the internal charge and field evolution. The existing code configuration relies on macroscopic phenomenological descriptions of some of the important dielectric processes (e.g., bulk conduction is treated with an empirically determined conductivity model). Work is currently underway to include a detailed carrier statistics package into the code description of the trapping.

After introducing the basic features of the model, code results are illustrated by a series of special case analytical solutions which rely on the basic transport calculations. The presentation utilizes the method of successive complication, i.e., the results proceed from the simplest to the most complicated by the successive relaxation of constraints. Because dielectric phenomena are generally so complicated, we believe this method to be essential for isolating those ingredients of the model which are critical. Future research may then focus on these critical areas.

The analytical results are followed by completely numerical computations for cases which are too difficult to handle analytically. All of the sample calculations suggest that the front face electric field arising from the charge separation of the deposited electrons and the secondary emission electron depletion region is well below expected breakdown fields. As these results are not in keeping with the Meulenberg discharge hypothesis (ref. 12),

we pinpoint the assumptions which give rise to our results, discuss limitations of the calculations, and suggest experiments which may be useful in determining the range of validity of our predictions.

ONE-DIMENSIONAL MODEL

Shown in figure 1 is the basic one-dimensional model which is assumed throughout this paper. We have chosen this model for several reasons. Our primary concern is with the conditions which occur internal to the dielectric. The indicated dielectric geometry provides the simplest configuration which can be investigated. This geometry has the advantage of isolating the physical effects occurring within the dielectric from complicated multi-dimensional effects due to transverse currents and fields. Additionally, it is expected that a one-dimensional treatment of the dielectric is an excellent approximation over most of the dielectric area. That is, away from edges, corners, holes, etc., the external conditions vary slowly transverse to the surface compared to variations through the sample (variations in mils or less). Relating the incident spectrum and primary current J_I to the source spectrum and current J_∞ in one dimension is not generally justified. For a realistic satellite configuration, this relationship can only be extracted by using a three-dimensional code of the NASCAP type (ref. 10). Recognizing this, we have established our computational algorithm so that it will accept an incident spectrum and current from other sources. The specific relationship implied by figure 1, however, is itself useful. Most laboratory simulation arrangements attempt to achieve this simple configuration to some degree. The computed results may be directly compared to the data from these configurations to obtain meaningful information. The additional merit of the configuration is that complicated multi-dimensional effects do not obscure the attempt to understand the basic charging process.

Several additional simplifications should be noted. It is assumed that the beam energy and current density and the model dimensions are such that

(1) the potential does not change significantly during an electron transit time, and

(2) that space charge effects in the vacuum are negligible.

For laboratory applications in the regimes of interest to spacecraft charging, these assumptions are true to a very high degree of accuracy. Under these conditions, the current density is constant throughout the vacuum region. We also assume that the source current is constant in time throughout this paper. While there are undoubtedly interesting effects which may be studied by modulating the beam current, we felt it best to initiate our studies with the customary laboratory condition of constant current. The code version of the model, SCCPOEM, easily accepts time-dependent currents. We do, however, explicitly consider two separate time histories for the source spectrum. We arbitrarily designate these as the "normal" and "feedback" cases. The "normal"

case corresponds to the typical experimental circumstances in which the source spectrum is constant. The "feedback" case is distinguished by having an incident spectrum that is constant. Experimentally, this would correspond to applying an additional accelerating voltage to the source spectrum which exactly cancels the retarding potential of the charged surface. From an analytical point of view, this condition has the merit of maintaining constant source terms. Experimentally, this configuration could be useful for studying the dependence of important charging quantities (backscatter and secondary currents, for example) on the sample voltage and charging history.

Our notation for a number of the primary quantities, and our choice of spatial coordinate system is given in Figure 1. The capacitance (per unit area) of the dielectric surface to the left hand plate (∞) C_o is related to the distance to the surface L by $C_o = \epsilon_o/L$, while the sample capacitance C_D is related to the sample thickness δ by $C_D = \epsilon/\delta$ (ϵ_o and ϵ are the permittivities of the vacuum and dielectric, respectively). For laboratory conditions C_o (capacitance to tank) is normally determined by a dimension somewhat smaller than the distance to the electron source. Generally, however, the condition $C_o << C_D$ holds. We still often find it convenient to eliminate the dependence of the solution on this laboratory dimension, and will take $C_o = 0$ (with appropriate limits). The equations describing the basic charging process are well known and have been documented elsewhere (ref. 17) for the model presented here. They are presented as needed in the course of the text.

THICK SAMPLES — EXTERIOR CHARGING VARIABLES

The external charging process may be characterized by a simple circuit model. The equations of the model are

$$C_o \frac{dV_o}{dt} = \bar{J}_o - \bar{J} \tag{1}$$

$$C_D \frac{dV_D}{dt} = \bar{J}_D - \bar{J} \tag{2}$$

where V_o is the potential drop from the left hand plate to the surface, V_D is the drop from the surface to the right hand plate, and the other symbols have the meanings noted above. Equations (1) and (2) are a rigorous consequence of the Maxwell equations. During the normal laboratory charging operation, the sample plate is connected to ground using a low value resistor, so that effective short circuit boundary conditions are the rule ($V_o + V_D = 0$). We consider this case exclusively throughout. Under these conditions, the external (short-circuit) current $\bar{J}$* is given by

*To avoid repetition, we refer to current densities as currents, with the area implied.

$$\bar{J} = \frac{C_D}{C}\bar{J}_o + \frac{C_o}{C}\bar{J}_D \qquad (3)$$

where $C = C_o + C_D$ is the total capacitance (parallel) of the sample surface to ground. The charging rate of the surface potential (V_o) is then determined by

$$C\frac{dV_o}{dt} = \bar{J}_o - \bar{J}_D \qquad (4)$$

which is the equation previously used by Purvis, et al. (ref. 18).

Internal to the dielectric the electric field satisfies the one-dimensional equation of Poisson:

$$\frac{dE}{dx} = \rho/\varepsilon \qquad (5)$$

where ρ is charge density in the dielectric. Let Q be the total charge (per unit area) in the dielectric. Integration of equation (5) yields the result

$$Q = \frac{\varepsilon(1 + \delta/L)}{(\delta - \bar{x})} V_o \qquad (6)$$

where $\bar{x}$ is the mean depth of the charge in the dielectric,

$$\bar{x} = \frac{\int_o^\delta \rho(x)x\,dx}{Q} \qquad (7)$$

If the inequality $\bar{x} << \delta$ holds throughout the charging, then $\bar{x}$ may be neglected — the voltage is determined by the geometric capacitance of the surface. Under these circumstances, the electric field is uniform throughout most of the sample, and a bulk conductivity may be used to characterize the conduction current through the volume. Thus, the conduction current $\bar{J}_D$ in equation (4) may be replaced by GV_o, where G is the conductance per unit area. These observations have been made numerous times and represent the standard approximation for use in higher dimensional codes of the NASCAP variety (ref. 13).

The point of this rather obvious exercise is that for thick samples ($\bar{x}<<\delta$) the quantities normally measured in charging experiments are effectively decoupled from the charge distribution which determines the electric field in the deposition region. This means that these measurements are unlikely to provide direct information about how the charge and fields are distributed in the surface layer.

Shown in figure 2 are the range and mean penetration of normally incident electrons in Teflon. Assuming that the electrons are trapped upon deposition in the material (which is true for small enough charge densities), we can see that even for 20 keV (3.2×10^{-15} joules) electrons, the mean penetration of 2 microns (2×10^{-6} m) is significantly smaller than the thickness of most spacecraft dielectrics (25 - 125 μm). If significant rearrangement of the charge does not occur via very low energy transport processes, then we may expect that this simple circuit model of the charging should adequately represent the internal charging measurements. This is the approach which was previously pursued by Purvis, et al. (ref. 18).

Let us assume that the secondary and backscatter yields from the dielectric do not depend on the surface voltage or charging history of the sample, but are a function only of the incident electron energy spectrum. Then the spatial current $\bar{J}_c$ is a function only of the source energy spectrum and the sample voltage. From above, the dielectric current $\bar{J}_D$ equals GV_o, where, in general, the conductance G is a function of V_o. The solution in this case may be reduced to quadrature:

$$\frac{t}{C} = \int_0^{V_o} \frac{dV'}{(\bar{J}_o(V') - GV')} \tag{8}$$

The relation implied by equation (8) must be inverted to provide the voltage as a function of time. Because the integral is not normally expressible in terms of tabulated functions, the direct numerical solution of equation (4) as performed by Purvis, et al. (ref. 18) is usually preferable.

Several simply expressible cases are worth noting. They are not unrealistic and provide excellent checks on numerical solutions. Let the conductance be independent of field strength, and let $\bar{J}_o$ be constant ("feedback" case). In this case V_o is given by

$$V_o = \frac{\bar{J}_o}{G}\left(1 - \exp(-\frac{G}{C}t)\right) \tag{9}$$

Shown in figure 3 is the backscatter yield Y_{BS} from Teflon as computed by SCCPOEM. It is reasonable to choose this quantity to be constant over the range of interest (2 - 20 keV)(3.2 - 32 x 10^{-15} J). Also shown in figure 3 are two representations of the secondary yield curve for normally incident electrons on Teflon as compiled by Wall, et al. (ref. 19), one using the Sternglass fit (ref. 20), and the other using a power law fit of Burke, et al. (ref. 21). An intermediate representation which varies inversely with electron energy is also sketched. If we use this very crude intermediate representation of the secondary yield for a constant conductivity dielectric, then the integral in equation (8) may easily be resolved for the "normal" case of monoenergetic electrons. Let the secondary yield Y_s have the form $Y_s = A/E_I$,

where E_I is the incident electron energy. The time history of the charging is described by the equation

$$2\frac{G}{C}t = \left(\frac{E_+ + E_-}{E_+ - E_-}\right) \ln\left[\frac{(E + eV_o - E_-)(E - E_+)}{(E + eV_o - E_+)(E - E_-)}\right]$$

$$- \ln\left[\frac{(E + eV_o - E_-)(E + eV_o - E_+)}{(E - E_+)(E - E_-)}\right] \tag{10}$$

where

$$E_\pm = (2G)^{-1}\left\{GE - e(1 - Y_{BS})\, J_\infty \pm \left[\left(GE - e(1 - Y_{BS})\, J_\infty\right)^2 + 4eGAJ_\infty\right]^{1/2}\right\} \tag{11}$$

e is the electronic charge, E the source energy, and Y_{BS} the backscatter coefficient.

The potential to which the sample will charge is obtained by setting the charging current to zero, i.e.,

$$\overline{J}_\sigma = GV \tag{12}$$

which is a special case of the charging equation which has been traditionally used in the spacecraft charging community. The equation is, in general, a transcendental equation which may be solved by standard relaxation techniques. For the "feedback" current source the solution is simplest. Shown in figure 4 is the final voltage for the "normal" case of normally incident monoenergetic electrons on Teflon, assuming a constant bulk conductivity of 3.3×10^{-16} mho/m (S/M). Note that the solution depends only on the ratio $(\sigma/\delta J_\infty)$, so solutions for other values of σ may be obtained by scaling. The solution shown in figure 4 assumes the correct power law fit of figure 3 for the secondary yield. For small currents, the charging is stopped by leakage currents while for large source currents, the charging is stopped by secondary emission.

INTERNAL FIELDS — MONOENERGETIC NORMALLY INCIDENT SOURCES

We have seen above that for thick samples the external variables are effectively decoupled from the internal variables. It is our primary interest to understand the internal fields in the thin surface layer in which the charge deposition takes place. In this section we give expressions for these fields under various special circumstances for monoenergetic normally incident source electrons, the customary laboratory configuration. It will be assumed throughout that secondary emission occurs from a layer which is much thinner ($\sim 10^{-9}$ m) than the primary deposition layer (at least 10^{-7} m). The positive depletion region will appear as a surface charge.

Shown in figures 5 and 6 are the charge deposition and dose profiles calculated by SCCPOEM for normally incident monoenergetic electrons on Teflon. Note the significant spread in both of these quantities. We will assume throughout this section that these primary electrons are trapped in the spatial region where they thermalize and that all charge relaxation occurs via conduction mechanisms. Carrier dynamics will be discussed in future work.

NON-CHARGING BEAM

Assume that the primary beam energy is such that the secondary plus backscatter current equals the incident current ($E \sim 2.5$ keV) (4×10^{-16} J). Under these circumstances, the surface potential remains identically zero, while $\bar{J}_o = \bar{J} = 0$. The current in the dielectric is given by $J_p(x) + \sigma(x)E$, where J_p is the current due to the incident electrons, and $\sigma(x)$ is the local conductivity (which we assume may depend on x, but not E). The internal electric field E is given by

$$E(x,t) = -\frac{J_p(x)}{\sigma(x)}\left(1 - \exp\left(-\frac{\sigma(x)}{\epsilon}t\right)\right) \tag{13}$$

The primary current J_p is proportional to the incident current $J_p(x) = Y(x)J_I$, where Y(x) is the current profile. Suppose that $\sigma(x)$ is the ambient conductivity. Under these conditions, the asymptotic field will scale with J_I, indicating that breakdown would always occur if the beam current were large enough. In the regions of interest, however, dielectric conductivity is dominated by the radiation induced conductivity (driven by the primary electrons) in the primary deposition region. This conductivity has the empirical form (ref. 22):

$$\frac{\sigma}{\epsilon} = K_p \dot{D}^{\Delta} \tag{14}$$

where K_p and Δ are empirically determined constants, and $\dot{D}$ is the dose rate in the medium. Experimentally, Δ is found to be in the range $1/2 \leq \Delta \leq 1$, with contemporary opinion favoring unity as the correct value. Since the dose rate

is proportional to the incident current, for any value of Δ less than unity, larger and larger fields may be driven in the dielectric by using larger and larger current densities. For Δ equal to unity, the asymptotic field is independent of J_I, and is given by

$$E = \frac{Y(x)}{\epsilon K_p R(x)} \tag{15}$$

where R(x) is the dose profile in the medium.

The spatial dependences of the field and charge density are shown for Teflon in Figure 7 using a value of $K_p = 1.68 \times 10^{-5}$ $(Rads)^{-1}$ (1.68×10^{-3} $(Gy)^{-1}$) (ref. 23). The field scales inversely with K_p. The peak field appears at the front face of the dielectric. The potential drop ΔV across this charge separation region is obtained by integrating equation (15). It is related to the mean field $\bar{E}$ by $\bar{E} = (\Delta V)d$, where d is the thickness of the charge trapping region. Clearly, within this model, the value of the conductivity constant is critical in determining whether the fields become sufficiently high for breakdown to occur. Using the range of values quoted by Wall, et al. (ref. 19), we have computed the expected range of fields in this layer for Mylar, Kapton, and Teflon. These results are shown in Table 1.

With the possible exception of the maximum field for Kapton ($\sim 10^8$ V/m), these fields are nowhere near breakdown fields. One mil samples of the three materials have very similar breakdown strengths of about 3×10^8 V/m. Further, this strength increases with decreasing thickness. In particular, for the 1000 Å (10^{-7} m) charging depth of this problem, the maximum potential drop of only six volts would make it appear very unlikely that breakdown can occur for any of these materials under the given irradiation condition.

The time required to reach this saturation field depends on the incident current. For Teflon, with a 1 nA/cm^2 (10^{-5} A/m^2) beam, $K_p = 1.68 \times 10^{-5}$ $(Rads)^{-1}$ (1.68×10^{-3} $(Gy)^{-1}$) (ref. 23), the dielectric relaxation time $\tau = \epsilon/\sigma$ has a value of 7.7 sec. This quantity scales inversely with beam current and dielectric conductivity coefficient. Thus, the smaller value of K_p quoted in the literature (ref. 19) (e.g., Mylar) could have relaxation times as long as 125 sec at a beam current of 1 nA/cm^2 (10^{-5} A/m^2). None of these times is especially long compared to laboratory irradiation times.

"FEEDBACK" CONTROLLED CHARGING BEAM

For this case, the incident beam energy and current are constant. A reasonable assumption is that the secondary and backscatter emission are also constant, so that $\bar{J}_o$ is likewise constant. (Note that this type of experiment would be ideal for checking this assumption.) The primary dose and charge deposition profiles will also be constant in time. These simplifications make the problem analytically tractable. If we assume that the conductivity is independent of electric field, then an exact solution may be given. The method of solution requires the application of LaPlace transforms, a method we have used elsewhere (ref. 24) for a similar problem. This solution is extremely

unwieldy and will not be detailed herein. Instead, we note that if $C_o = 0$, then further simplification occurs. Corrections to the solution for finite C_o are of order C_o/C_D, so that the approximate solution is an excellent representation of reality for most laboratory configurations. With these assumptions, we find the following expression for E:

$$E(x,t) = \frac{[\bar{J}_o - J_p(x)]}{\sigma(x)} [1 - \exp(-\frac{\sigma(x)}{\varepsilon} t)] \tag{16}$$

Note that this solution does not depend on the thick sample assumption. If we consider the primary deposition region only ($J_p \neq 0$), then the solution is identical to that given previously, except that $(\bar{J}_o - J_p)$ is the current profile of interest. Note that the electric field profile now changes sign as was first pointed out by Meulenberg (ref. 12). For incident energies such that $|\bar{J}_o - J_p(0)| > |\bar{J}_o|$, the peak electric field can occur at the front face while for the reverse inequality, the peak field is always in the bulk. In the bulk, the electric field is given by $\bar{J}_o/\sigma_o$, where σ_o is the bulk conductivity, so that E_{BULK} may be made arbitrarily large by increasing the incident current.

At the front face $J_p(0) = (1 - Y_{BS})J_I$ and $\bar{J}_o = (1 - Y_S - Y_{BS})J_I$, where Y_S, Y_{BS} are the secondary and backscatter yields, respectively. Thus, at saturation, the front face field E_{FF} is given by

$$E_{FF} = -\frac{Y_S J_I}{\sigma(0)} \tag{17}$$

For sufficiently large currents ($>10^{-8}$ A/m^2), the radiation-induced conductivity completely dominates the ambient conductivity, so that $\sigma(0)$ takes the radiation-induced value. With a conductivity of the form of equation (14), we again note that E_{FF} may take on arbitrarily large values for sufficiently large currents if $\Delta < 1$. For the case that Δ has the value unity, the value of the front face field is independent of the current. Moreover, if we use the fit of Burke, et al. (ref. 21) to the secondary emission yield shown in figure 3, we find that E_{FF} is also independent of the primary beam energy. This occurrence will be discussed in further detail below. The maximum value of the front face electric field for Teflon, Mylar, and Kapton may be obtained from the maximum values given in Table 1. These occur for the minimum value of K_p. A use of the Sternglass fit (ref. 20) to the secondary yield shown in Figure 3 would result in smaller fields.

GROUNDED FRONT FACE

Another case of interest occurs when the front face of the dielectric is coated with a thin layer (compared to an electron range) of conductor, and the conductor is grounded to the sample backside. This situation also effectively occurs when sunlight is present on the sample, so that a plethora of photoelectrons are available to keep the sample from charging. The general solution

for the time dependence of this problem has been given by us elsewhere (ref. 24). It involves LaPlace transforms and is rather complicated, so it will not be repeated here. The saturation field, however, has a simple form, given by

$$E = \frac{\bar{J} - J_p(x)}{\sigma(x)} \tag{18}$$

where

$$\bar{J} = \frac{\int_0^\delta dx \, \frac{J_p(x)}{\sigma(x)}}{\int_0^\delta dx \, \frac{1}{\sigma(x)}} \tag{19}$$

and $J_p(x)$ is the primary current profile in the medium. From equation (19), we can see that the short circuit current $\bar{J}$ is of order $J_p(\bar{x}/\delta)$, where $\bar{x}$ is the mean penetration. Thus, for thick samples $\bar{J}$ is small compared to J_p. The largest front face field occurs for $\bar{J} = 0$ and has the value $-(J_p(0) \div \sigma(0))$. Specializing to the case where conductivity is proportional to dose rate (our above remarks hold for $\Delta < 1$), this field is again independent of current. Shown in figure 8 is the stopping power for electrons in Teflon as a function of energy. For normally incident electrons, the surface dose also has this shape, decreasing for increasing energy. Because the backscatter yield is essentially constant in this regime (figure 3), $J_p(0)$ is essentially constant. This means that the front face electric field is an increasing function of the primary beam energy. This is illustrated in figure 9 for Teflon, Mylar, and Kapton using the minimum values of K_p quoted in Table 1. A comparison of these values with those given above, and in sections below, shows that grounding the face has made the front face field larger. Of course, the bulk fields are severely reduced.

"NORMAL" CHARGING BEAM

The case considered in this section represents the conventional laboratory charging condition of a monoenergetic normally incident source for which the source energy is constant in time. As the sample charges, the incident electron energy decreases, and the dose and charge deposition profiles vary as illustrated in figures 5 and 6. This situation appears too complicated for analytical attack. We illustrate the numerical solution given by SCCPOEM for 5 mil (1.27×10^{-4} m) Teflon. The secondary yield algorithm used takes the yield proportional to the dose as suggested by Burke, et al. (ref. 21). For normally incident electrons, this reproduces the power law fit given in figure 3. The bulk conductivity was taken from the data of Adamo and Nanevicz (ref. 25). The transient conductivity was taken proportional to the dose rate, with a coefficient of $K_p = 1.68 \times 10^{-5}$ (Rads)$^{-1}$ (1.68×10^{-3} (Gy)$^{-1}$) (ref. 23).

With these inputs, it is found that the surface charges to the voltage given in figure 4. The time dependence of the voltage and current histories are qualitatively similar to the data presented by Purvis, et al. (ref. 18). Quantitatively, the calculations show a slower charging than the data, and the calculated saturation current is far less than measured. As noted by Purvis, et al. (ref. 18), these discrepancies are probably due to capacitive fringing effects and surface leakage current. Artificially decreasing the capacitance and increasing the bulk conductivity gives solutions which adequately represent the data.

Shown in figure 10 is the time dependence of the electric field profile for a 12 keV (1.92×10^{-15} J) 1 nA/cm^2 (10^{-5} A/m^2) charging beam. It should be noticed that the front face field is already at its saturation value at the first time plot (t = 50 sec). The bulk field evolves to its final value as V/δ, where V is given by the external charging variables. Shown in figure 11 is the saturation field in Teflon as a function of the primary beam energy. Note that the field near the front face is identical for all the charging energies, while the magnitude of the bulk field reflects the equilibrium voltage shown in figure 4.

It certainly makes sense that the fields near the front face are identical, because as external saturation is reached, the incident electrons take on very nearly the same energy. For later time, this corresponds to constant J_0, dose and charge deposition profiles. The solution is then easy to demonstrate explicitly by using the internal equilibrium condition $\bar{J} = J$ but will not be pursued further here. What may perhaps be more surprising to the reader is that the value of the front face field shown in these figures is, in fact, a much more general result. This will be shown below after discussing several further examples.

INTERNAL FIELDS — OTHER SOURCES

The charging conditions which can occur are more general than those discussed above. These include the complications due to angular dependence in the source spectrum, as well as energetically distributed sources. While our charging geometry is much less realistic for these more general source configurations, it is instructive to briefly indicate these effects.

MONOENERGETIC ISOTROPIC SOURCE

Shown in figure 12 are the voltage time histories of 5 mil (1.27×10^{-4} m) Teflon subjected to normally incident and isotropically incident 20 keV (3.2×10^{-15} J) electrons. The saturation electric fields are compared in figure 13. The isotropic source charges much more slowly and reaches a significantly smaller voltage. This result occurs because both the backscatter and secondary yields are significantly higher for the isotropic source. Internally, the fields close to the front face evolve slowly (following the voltage curve of figure 12). Note that the front face field for the isotropic source is identical to the front face field for normally incident sources.

ISOTROPIC MAXWELLIAN SOURCE

We have computed the electron transport for a 10 keV (1.6×10^{-15} J) isotropic Maxwellian distribution. The backscatter yield was determined to be 0.34, while the secondary yield was determined to be 1.55. Thus, it is expected that the Teflon will charge positively. The code is not equipped to handle this possibility. The plethora of secondaries mean that the sample will charge to a few volts positive in a very short time, the exact value of the voltage depending on the secondary electron distribution. The voltage will adjust to make the net current to the surface zero. So far as the internal fields are concerned, this is precisely the case described above as the "non-charging" beam (similarly, the grounded front face situation). Thus, the internal electric field is given by equation (13). Our numerical results indicate a broad positive charge layer ($\sim$1 μm) near the front surface and a deeply buried negative charge. We are still investigating the correctness of this pecularity.

GENERAL FRONT FACE FIELD

The appearance of a single value for the front face field under a number of circumstances suggests a universality of this value within our computational model. This is indeed the case. The following considerations hold for charging conditions which result in a negative voltage (not artificially grounded). The field at the surface satisfies...

$$\frac{\partial E}{\partial t}(o,t) = \frac{\bar{J} - J(o,t)}{\epsilon} \tag{20}$$

For the case of vanishing tank capacitance ($C_o = 0$), $\bar{J} = \bar{J}_o$. The current in the dielectric consists of the primary current J_p and the conduction current σE. At the surface $\bar{J}_o - J_p(o) = -J_{BS}$, so that equation (20) becomes

$$\frac{dE}{dt}(o,t) + \frac{\sigma(o)}{\epsilon} E(o,t) = -J_{BS}(t) \tag{21}$$

The primary assumption of the computational model is that the backscatter current is proportional to the surface dose rate ($-J_{BS} = \alpha\dot{D}$) and the conductivity is proportional to dose rate ($\sigma = \epsilon K_p \dot{D}$). With these two assumptions, the surface field solution is

$$E(o,t) = \left(\frac{\alpha}{\epsilon K_p}\right)\left(1 - \exp\left[-K_p D(t)\right]\right) \tag{22}$$

Thus, the field takes on a value determined only by the dose and saturates to a universal material dependent value ($\alpha/\epsilon K_p$). This value is that given in Table 1 and is independent of the charging spectrum and time history.

FIELD DEPENDENT PRIMARY TRANSPORT

For completeness, we have performed the primary electron transport, including the effect of the internal electric fields on the electron motion. The effect was found to be completely negligible. A glance at figure 8 makes this easy to understand. The minimum value of the stopping power [for 20 keV (3.2×10^{-15} J) electrons] (in electric field units) is 2×10^9 V/m. Since the maximum fields encountered in these calculations are a few times 10^8 V/m, the fields have, at most, a 10% effect. For "normal" charging conditions, the effect is far less than this maximum, because of the sharp rise in stopping power for lower electron energies and the small value of the front face field.

CONCLUSIONS

We have presented a detailed model of the charging of dielectrics due to incident electrons. The computer model (SCCPOEM) as currently configured does not include the following effects:

- sunlight effects
- thermal effects
- ionic effects
- multi-dimensional effects
- field and charging history dependent secondary emission effects
- detailed carrier statistics effects, and
- very long time effects

The first four of these limit the applicability of the code to specialized charging situations but do not constitute limitations of principle.

The code presently chooses the secondary emission coefficient to be proportional to the computed surface dose as suggested by Burke, et al. (ref. 21). While this algorithm may fail at low energy [below a kilovolt (1.6×10^{-16} J)], it appears consistent with the experimental data above this energy. It is possible, however, that the secondary emission depends on the surface fields and charge profile which develops [see, e.g., Dekker (ref. 26)]. Some evidence is being accumulated by Robinson (ref. 27) that this effect occurs under the conditions of interest. Should the effect be demonstrated to be important, it can readily be incorporated into the code. This is true because the secondary emission primarily affects the external charging algorithm and enters the internal calculations as a boundary condition.

The major matters of principle not currently handled by the code are the details of the carrier statistics and migration. Empirical models are being utilized for both the bulk conductivity and the radiation induced conductivity. This shortcoming is currently being rectified. A version of the code which incorporates a carrier kinetics description of the conduction process is being developed. In defense of our present treatment, however, it must be mentioned

that a model utilizing direct empirical data has a major advantage over a more fundamental approach. Typically, the quantities which are required for a kinetic approach are very poorly known. The empirical conductivity data, while reflecting all these more fundamental quantities, has the advantage of being a direct measure of the relaxation phenomena. If used in the proper domain, the only uncertainties are the direct uncertainty in the conductivity measurement itself. The major uncertainty of principle is the domain of applicability. A good way to determine this domain is to use the model, make predictions, and compare to experiment. We have chosen this path. Indications are that the model is satisfactory for reasonably thick samples with fields not too near breakdown.

Dielectrics subject to electrical stresses undergo persistent change over very long periods of time (many years). This type of effect is completely beyond the scope of our present model.

Within the above constraints, the model provides a simple and effective tool for computing internal fields and charge densities in electron-irradiated dielectrics. Our computations to date indicate the following:

- At low charging currents, the final voltage is limited by bulk conduction, while at high currents, the voltage is limited by secondary emission.
- Normal charging gives rise to a field reversal layer as suggested by Meulenberg (ref. 12) but does not appear to give breakdown level fields at the surface.
- Charging with normally incident electrons under conditions in which the voltage is secondary limited gives rise to similar field profiles near the front face independent of charging energy.
- Secondary limited charging gives rise to a "universal" material dependent front face field.
- Grounded coatings on the front face decrease the bulk field but give rise to enhanced fields at the front face.
- Strong internal fields can arise even in low voltage positive charging environments.
- Angular distributions of monoenergetic electrons give less severe internal fields than normally incident electrons.

The key assumptions which give rise to the above conclusions are

- The independence of the secondary yield on charging conditions (dependence on only the incident electron spectrum).
- The proportionality of the secondary emission current to the dose rate.
- The use of the empirical conductivity model of equation (14) with $\Delta = 1$.
- The value of the empirical transient conductivity constant K_t.

We note some experiments which may be performed to test our conclusions and some of the assumptions:

- "Feedback" controlled experiments can be used to check the constancy of the secondary emission current.
- High current "non-charging" beams may be used to check the linearity of the transient conductivity with dose rate.
- Charge density interrogation experiments of the type suggested by Sessler, et al. (ref. 28) may be performed to directly compare to predicted charge densities.
- Grounded front face experiments may be performed to compare to short-circuit current predictions and check for breakdown.
- Very thin sample experiments can be performed with conventional measurements to check the influence of internal charge location on external variables.

We believe experiments of the above type, coupled with a detailed investigation of carrier kinetics restrictions, should lead to further understanding of the dielectric charging process.

We are indebted to Dr. J. V. Gore for numerous discussions, as well as certain of the calculations which appear herein.

REFERENCES

1. Chadsey, W. L.: POEM, AFCRL Technical Report, TR-75-0324, 1975.

2. Nanevicz, J. E.; Adamo, R. C.; and Scharfman, W. E.: SRI International, final report, Contract No. F04701-71-C-0130, P. O. 126192, Project 2611, 1974.

3. Stevens, N. J.; Lovell, R. R.; and Klinect: Preliminary Report on the CTS Transient Event Counter Performance through the 1976 Spring Eclipse Season, in "Proceedings of the Spacecraft Charging Technology Conference," C. P. Pike and R. R. Lovell, editors, Air Force Surveys in Geophysics, No. 364, AFGL-TR-77-0051, NASA TMX-73537, 24 February 1977, p. 81.

4. Stevens, N. J., Berkopec, F. D.; Staskus, J. V.; Blech, R. A.; and S. J. Narcisco: Testing of Typical Spacecraft Materials in a Simulated Substorm Environment, ibid., p. 431.

5. Bogus, K. P.: Investigation of a CTS Solar Cell Test Patch Under Simulated Geomagnetic Substorm Charging Conditions, ibid., p. 487.

6. Robinson, J. W.: Charge Distributions Near Metal-Dielectric Interfaces Before and After Dielectric Surface Flashover, ibid., p. 503.

7. Balmain, K. G.; Cuchanski, M.; and Kremer, P. C.: Surface Micro-discharges on Spacecraft Dielectrics, ibid., p. 519.

8. Hoffmaster, D. K.; Inouye, G. T.; and Sellen, J. M., Jr.: Surge Current and Electron Swarm Tunnel Tests of Thermal Blanket and Ground Strap Materials, ibid., p. 527.

9. Amore, L. J. and Eagles, A. E.: Materials and Techniques for Spacecraft Static Charge Control, ibid., p. 621.

10. Nanevicz, J. E. and Adamo, R. C.: Spacecraft Charging Studies of Voltage Breakdown Processes on Spacecraft Thermal Control Mirrors, in Spacecraft Charging by Magnetospheric Plasmas, Vol. 47, Progress in Astronautics and Aeronautics, A. Rosen, editor, 1976, p. 225.

11. Yadlowky, E. J.; Hazelton, R. C.; and Churchhill: Characterization of Electrical Discharges on Teflon Dielectrics Used as Spacecraft Thermal Control Surfaces, paper V-2, this proceedings.

12. Meulenberg, A., Jr.: Evidence for a New Discharge Mechanism for Dielectrics in a Plasma, ref. 10, idem, p. 237.

13. Katz, I.; Parks, D. E.; Mandell, M. J.; Harvey, J. M.; Brownell, D. H., Jr.; Wang, S. S.; and Rotenberg, M.: A Three Dimensional Dynamic Study of Electrostatic Charging in Materials, NASA CR-135256, NASA Lewis Research Center, Cleveland, Ohio, 1977.

14. O'Dwyer, J. J.: The Theory of Electrical Conduction and Breakdown in Solid Dielectrics, Clarendon Press, Oxford, 1973.

15. Moh, N. F. and Davis, E. A.: Electronic Processes in Non-Crystalline Materials, Clarendon Press, Oxford, 1971.

16. Lampert, M. A. and Mark, P.: Current Injection in Solids, Academic Press, New York, 1970.

17. Beers, B. L. and Pine, V. W.: Electron Transport Model of Dielectric Charging, Interim Report, SAI-102-78-002, for Communications Research Centre, Ottowa, Ontario, Canada, Science Applications, Inc., 8330 Old Courthouse Road, Vienna, Virginia, 1978.

18. Purvis, C. K.; Stevens, N. J.; and Oglebay, J. C.: Charging Characteristics of Materials: Comparison of Experimental Results with Simple Analytical Models, ref. 3, idem, p. 459.

19. Wall, J. A.; Burke, E. A.; and Frederickson, A. R.: Results of Literature Search on Dielectric Properties and Electron Interaction Phenomena Related to Spacecraft Charging, ref. 3, idem, p. 569.

20. Sternglass, E. J.: Phys. Rev. 80, 1950, p. 925.

21. Burke, E. A.; Wall, J. A.; and Frederickson, A. R.: Radiation-Induced Low Energy Electron Emission from Metals, IEEE Trans. Nuc. Sci., NS-19, 1972 p. 193.

22. Fowler, J. F.: Proc. Roy. Soc. London, Ser. A236, 1956, p. 464.

23. Weingart, R. C.; Barlett, R. H.; Lee, R. S.; and Hofer, W.: X-Ray Induced Photoconductivity in Dielectric Films, IEEE Trans. Nuc. Sci., NS-19, 1972, p. 15.

24. Beers, B.: Radiation-Induced Signals in Cables - II, IEEE Trans. Nuc. Sci., NS-24, 1977, p. 2429.

25. Adamo, R. C.; Nanevicz, J. E.; and Grier, N.: Conductivity Effects in High-Voltage Spacecraft Insulating Materials, ref. 3, idem, p. 669.

26. Dekker, A. J.: Secondary Electron Emission, Solid State Physics 6, 1958, p. 251.

27. Robinson, J. W.: Stable Dielectric Charge Distributions from Field Enhancement of Secondary Emission, paper V-8, this proceedings.

28. Sessler, G. M.; West, J. E.: Berkley, D. A.; and Morgenstern, G.: Determination of Spatial Distribution of Charges in Thin Dielectrics, Phys. Rev. Lett. 38, 1977, p. 368.

TABLE 1. RANGE OF VALUES OF PEAK ELECTRIC FIELD FOR NON-CHARGING BEAM

Range reflects spread in quoted values of the Transient Dielectric Conductivity Coefficient K_p (ref. 19).

MATERIAL	PEAK ELECTRIC FIELD ($\times 10^6$ V/m)	MEAN ELECTRIC FIELD ($\times 10^6$ V/m)	POTENTIAL DROP (volts)
TEFLON	0.11 - 5.5	0.06 - 2.9	0.007 - 0.372
MYLAR	52. - 61.	28. - 32.	3.5 - 4.1
KAPTON	1.8 - 92.	1.0 - 49.	0.1 - 6.2

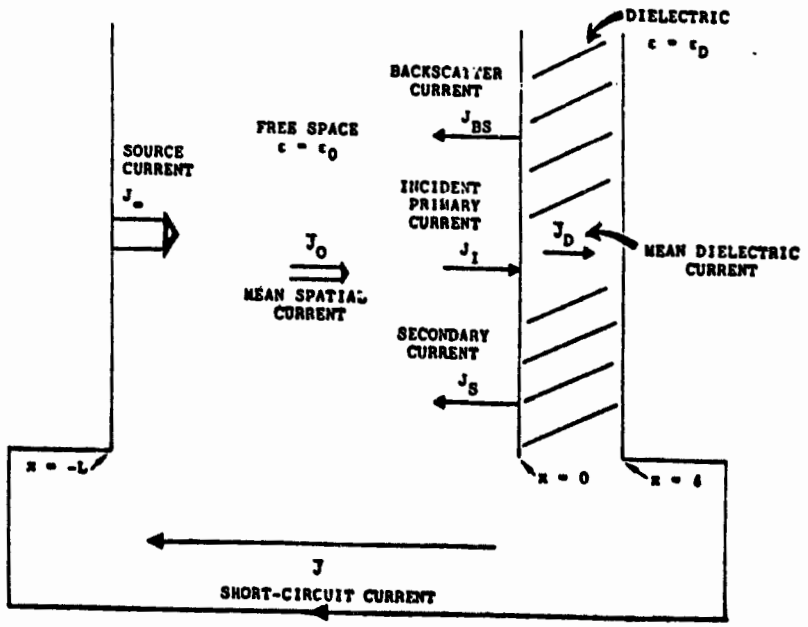

FIGURE 1. ONE-DIMENSIONAL CHARGING MODEL

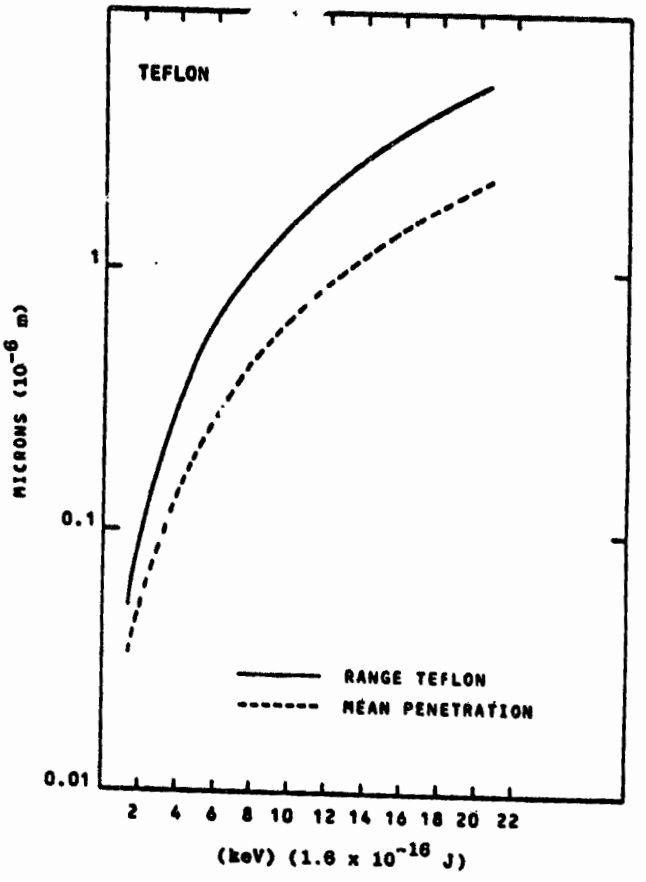

FIGURE 2. RANGE AND MEAN PENETRATION FOR NORMALLY INCIDENT ELECTRONS IN TEFLON

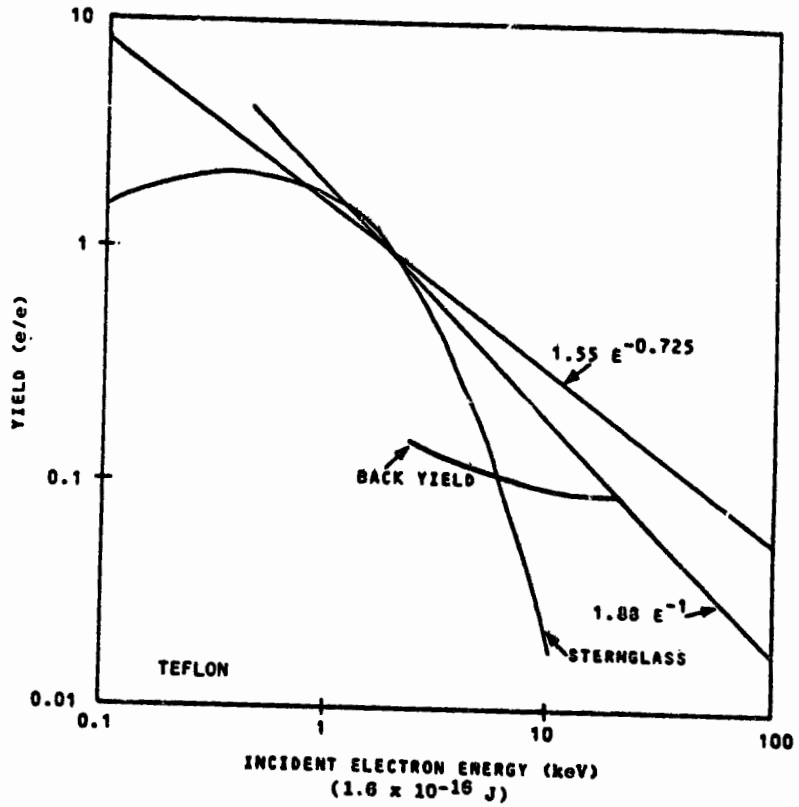

FIGURE 3. BACKSCATTER AND SECONDARY YIELDS FOR NORMALLY INCIDENT ELECTRONS ON TEFLON

SOURCES ARE CITED IN THE TEXT.

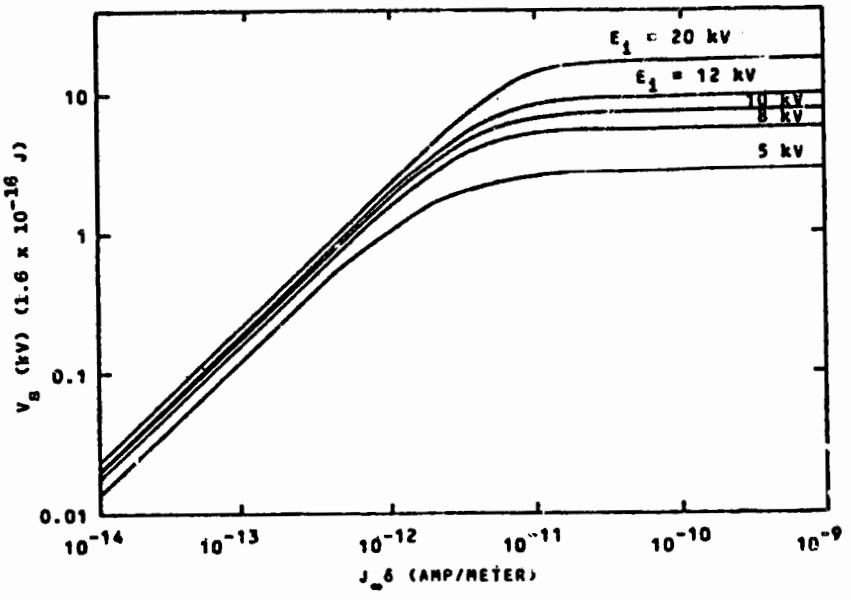

FIGURE 4. SATURATION CHARGING VOLTAGE FOR NORMALLY INCIDENT ELECTRONS ON TEFLON AS A FUNCTION OF THE CHARGING CURRENT DENSITY TIMES THE DIELECTRIC THICKNESS

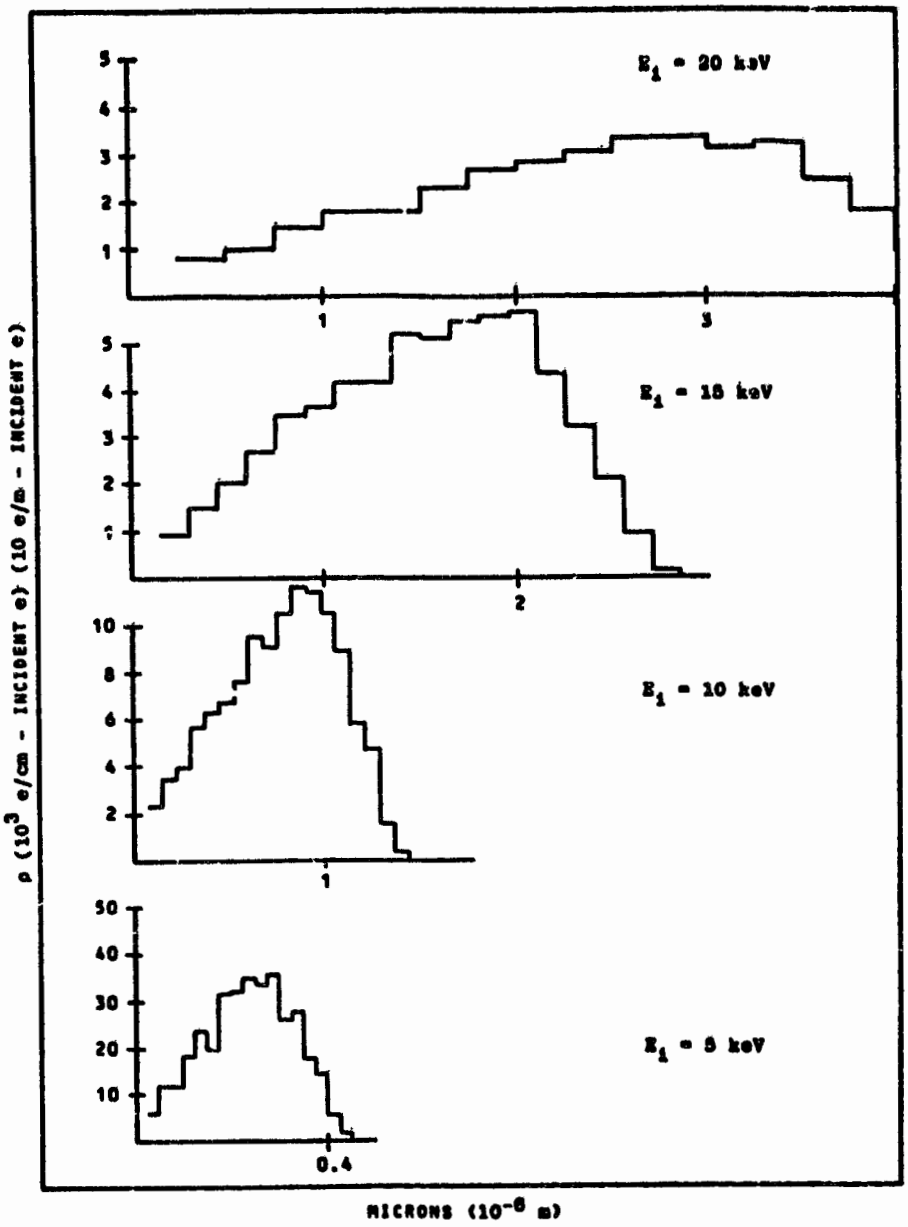

FIGURE 5. CHARGE DEPOSITION PROFILE IN TEFLON FOR NORMALLY INCIDENT ELECTRONS

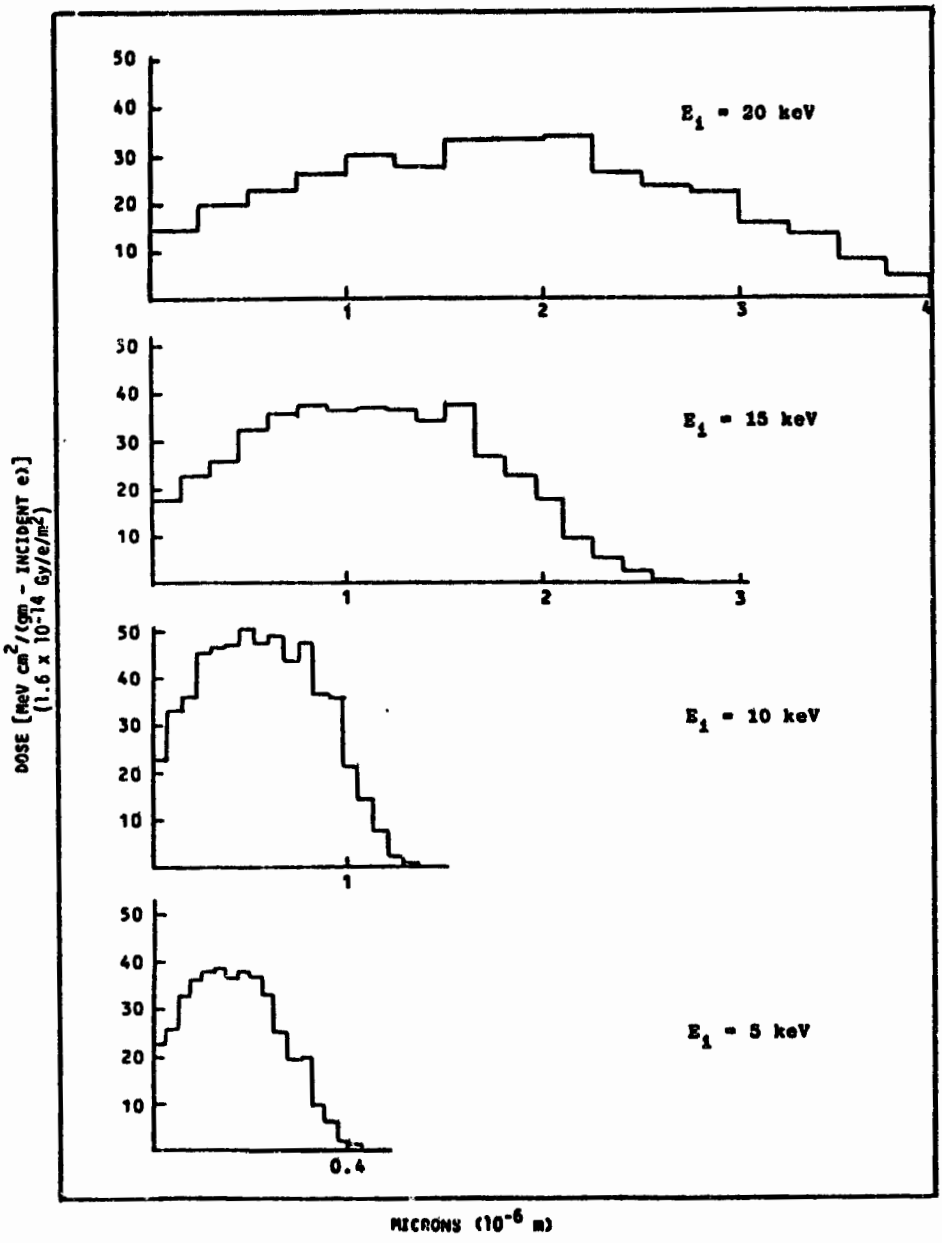

FIGURE 6. DOSE PROFILE IN TEFLON FOR NORMALLY INCIDENT ELECTRONS

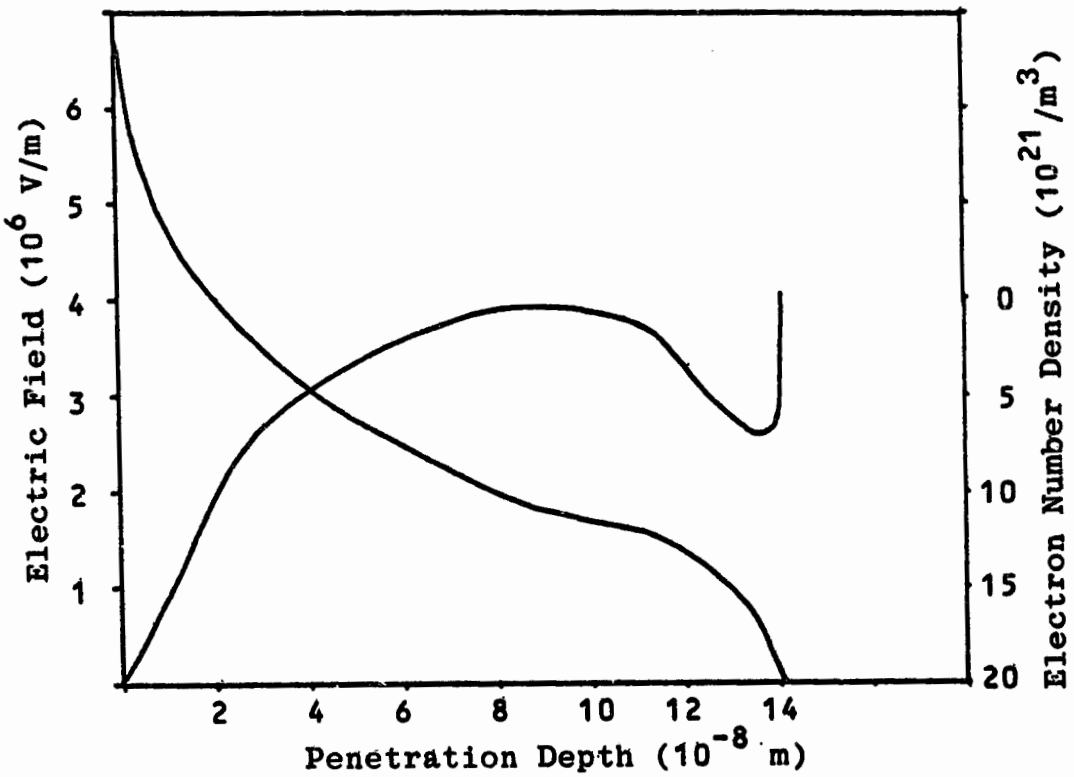

FIGURE 7. SATURATION ELECTRIC FIELD IN TEFLON FOR NON-CHARGING NORMALLY INCIDENT BEAM

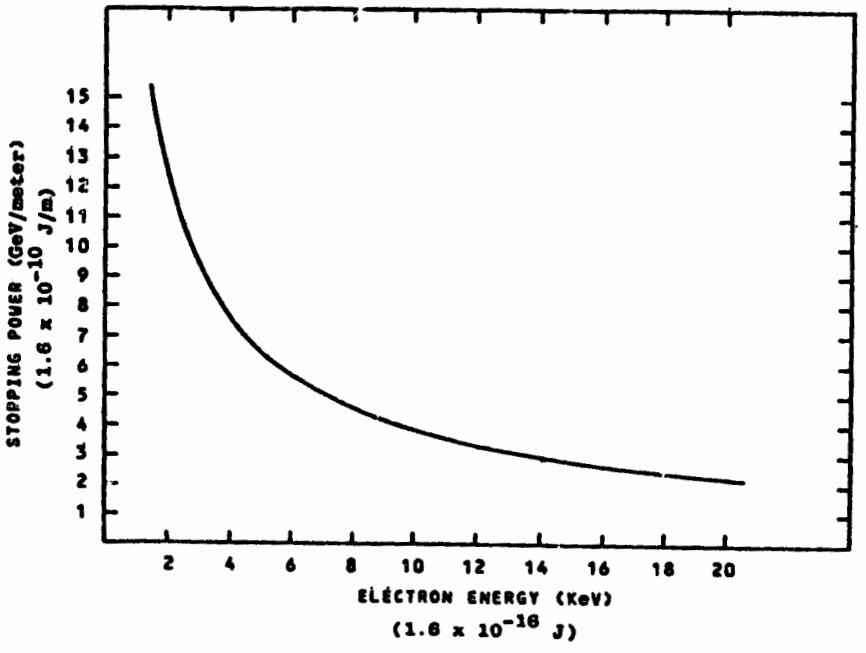

FIGURE 8. ELECTRONIC STOPPING POWER OF TEFLON

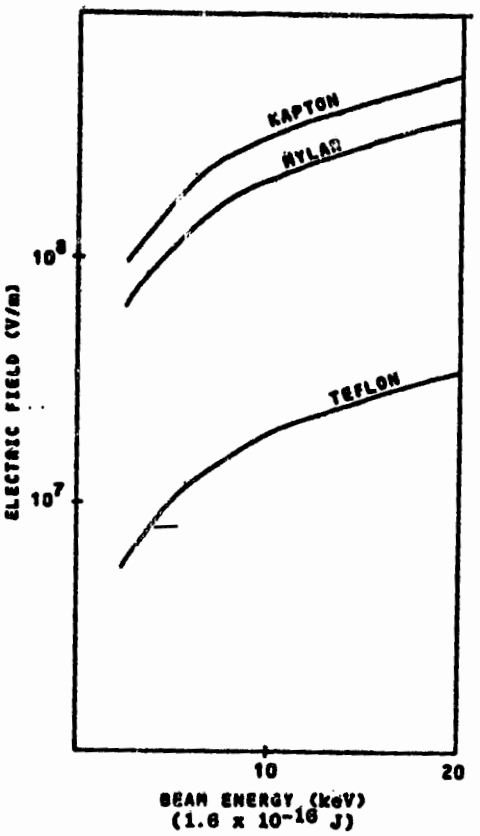

FIGURE 9. FRONT SURFACE SATURATION FIELD FOR GROUNDED FRONT-FACE - NORMALLY INCIDENT ELECTRONS - MINIMUM VALUE OF K_p

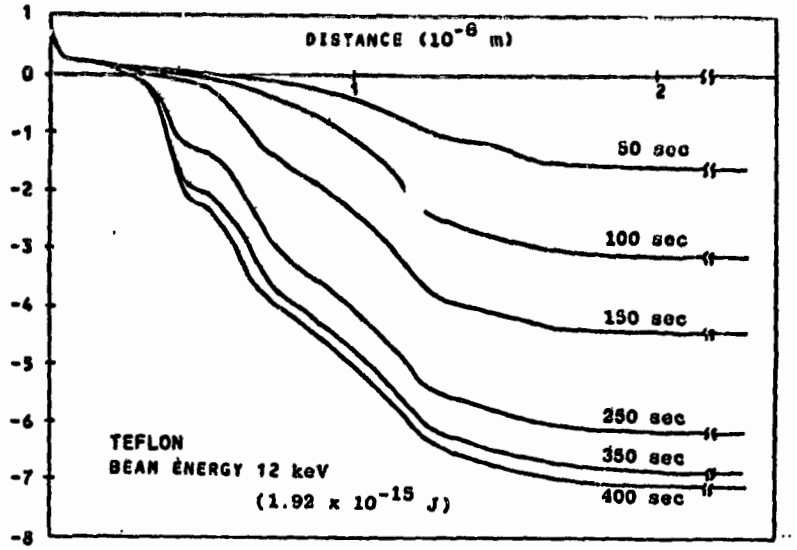

FIGURE 10. TIME HISTORY OF THE ELECTRIC FIELD PROFILE IN TEFLON - NORMALLY INCIDENT 12 keV ELECTRONS

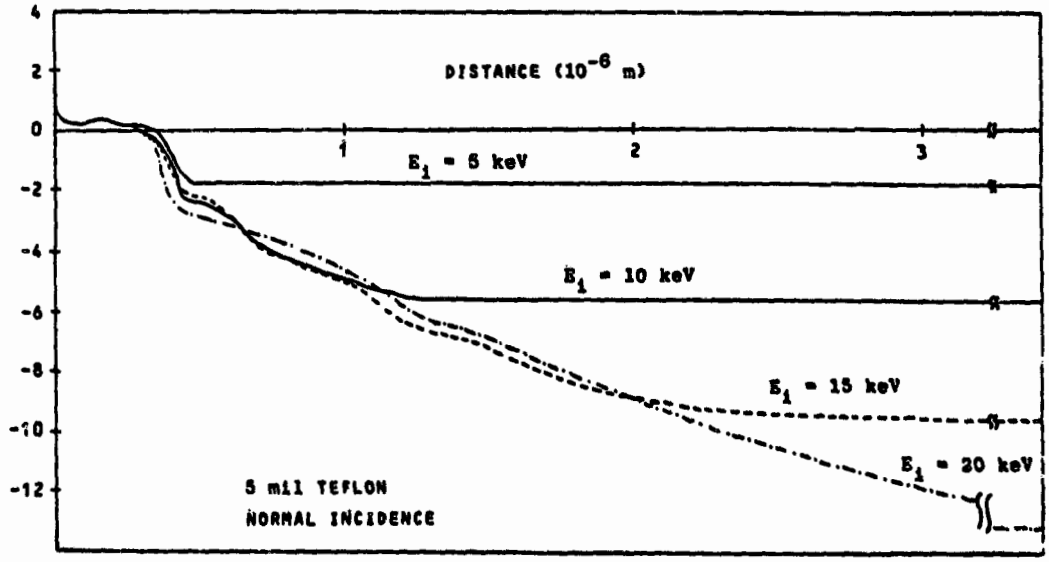

FIGURE 11. SATURATION ELECTRIC FIELD PROFILES IN 5 mil (1.27×10^{-4} m) TEFLON - NORMALLY INCIDENT ELECTRONS

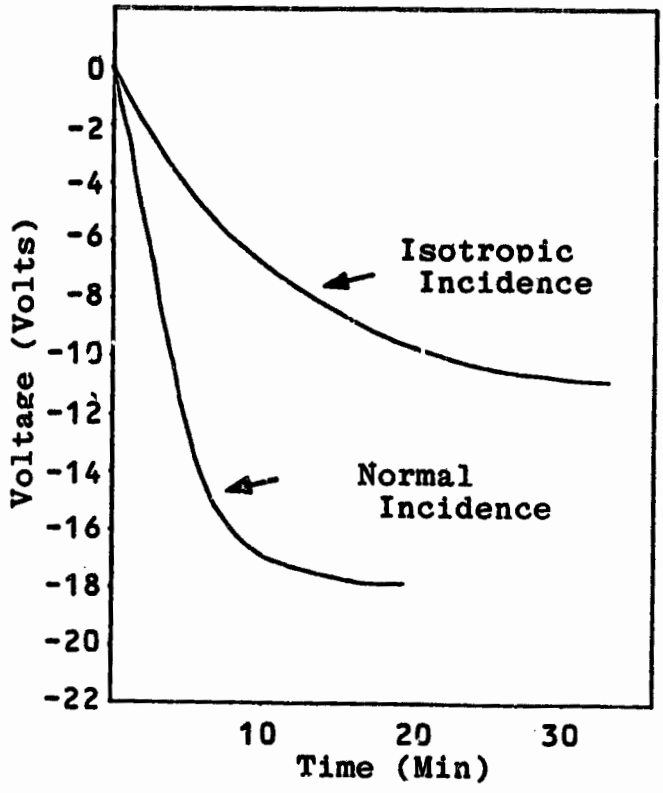

FIGURE 12. CHARGING VOLTAGE TIME HISTORIES FOR NORMALLY INCIDENT AND ISOTROPIC 20 keV ELECTRONS ON 5 mil TEFLON

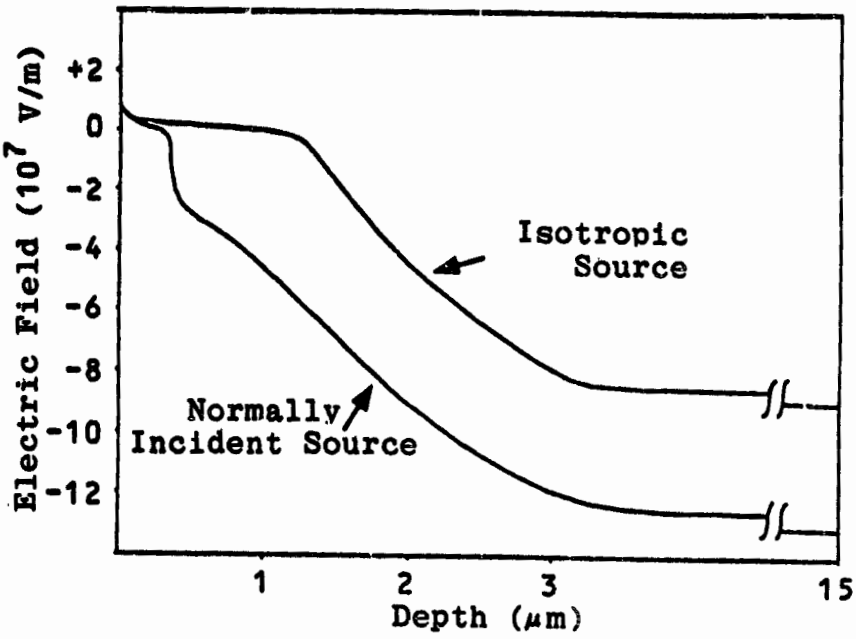

FIGURE 13. COMPARISON OF SATURATION ELECTRIC FIELD PROFILES FOR NORMALLY INCIDENT AND ISOTROPIC 20 keV CHARGING SOURCE — 5 mil TEFLON —